

Multigrid solver for axisymmetrical 2D fluid equations

Zoran Ristivojevic¹, Zoran Lj. Petrović¹

¹*Institute of Physics, University of Belgrade, P.O. Box 68, 11080 Zemun, Serbia*

We have developed an efficient algorithm for steady axisymmetrical 2D fluid equations. The algorithm employs multigrid method as well as standard implicit discretization schemes for systems of partial differential equations. Linearity of the multigrid method with respect to the number of grid points allowed us to use 256×256 grid, where we could achieve solutions in several minutes. Time limitations due to nonlinearity of the system are partially avoided by using multi level grids (the initial solution on 256×256 grid was extrapolated steady solution from 128×128 grid which allowed using “long” integration time steps). The fluid solver may be used as the basis for hybrid codes for DC discharges.

1. Introduction

Further understanding of basic processes in gas discharges and non-equilibrium plasmas relies on comparisons of experimental results and predictions of theoretical results which almost always have to be numerical calculations including self consistent calculation of the spatial profile of electric field. In all calculations it is critical to calculate the properties of electrons which have large mobility and consequently ability to gain energy from the electric field. Consequently electrons play a critical role in sustaining the plasma by gas phase ionization. At the same time electrons have non-local or non-hydrodynamic kinetics as their properties in the rapidly changing fields may not be defined uniquely by the local electric field. Thus, hybrid models were developed to take into account high energy electrons originating from the electrodes or created in very high electric fields close to the electrodes by using a Monte Carlo technique while the bulk of electrons at low energies is accounted for by a fluid model.

As the need to describe accurately more and more complex geometries transition from 1D to 2D and 3D systems becomes increasingly demanding in terms of computer time and complexity of equations that may lead to numerical problems such as numerical diffusion and others. In particular as the grid becomes denser the computational demands increase as a square or cube of the number of grid points. Thus, in order to model realistic structures and complex geometries with proper relaxation of high energy electrons in space and time, one needs to develop special numerical procedures to handle the complex task. In this paper we describe one implementation of the multigrid technique which is far proved to be the leading contender for optimal

treatment of 3D systems with a large number of grid points.

2. Fluid equations and numerical algorithm
Continuity equations for the electrons and the ions are [1]

$$\frac{\partial n_e}{\partial t} + \nabla \cdot (n_e \mathbf{v}_e) = S_e, \quad (1)$$

$$\frac{\partial n_p}{\partial t} + \nabla \cdot (n_p \mathbf{v}_p) = S_p. \quad (2)$$

Momentum balance equations are

$$\phi_e = n_e \mathbf{v}_e = -n_e \mu_e \mathbf{E} - D_e \nabla(n_e), \quad (3)$$

$$\phi_p = n_p \mathbf{v}_p = n_p \mu_p \mathbf{E} - D_p \nabla(n_p). \quad (4)$$

Electric potential is governed by the Poisson equation

$$\nabla^2 V = -\frac{e}{\epsilon_0} (n_p - n_e), \quad (5)$$

while the electric field is negative gradient of the potential:

$$\mathbf{E} = -\nabla V. \quad (6)$$

In previous equations subscript index e (p) refers to the electrons (ions). Input parameters for the fluid equations are source terms S_e and S_p , mobilities $\mu_e(\mathbf{E})$ and $\mu_p(\mathbf{E})$, diffusion coefficients $D_e(\mathbf{E})$ and $D_p(\mathbf{E})$ and are supposed to be known (e.g. in hybrid models they are provided from the lookup tables and Monte Carlo code).

We will solve a set of equations (1)-(6) for the azimuthal symmetry ($f(r, z, \Theta) = f(r, z)$) and for a given set of boundary conditions.

First we discretize system (1)-(6): we split the domain $(r, z) \in [0, R] \times [0, d]$ into rectangles with equidistant radial grid points r_0, r_1, \dots, r_{N_r} and non-equidistant axial grid points z_0, z_1, \dots, z_{N_z} . We also have midpoints between the grid points $r_{i+1/2}$ and $z_{j+1/2}$. In the following we use indices i, j, k for

r -coordinate, z -coordinate and for the time, respectively. In order to allow long integration times the system must be discretized implicitly in time [2]. Continuity equations (1) and (2) are discretized “backward in time”

$$\frac{n_{i,j}^{k+1} - n_{i,j}^k}{\Delta t} + (\nabla_r \phi_r)_{i,j}^{k+1} + (\nabla_z \phi_z)_{i,j}^{k+1} = S_{i,j}. \quad (7)$$

Momentum balance equations are of convection-diffusion type and it is convenient to discretize them by the Scharfetter–Gummel scheme [2]:

$$\phi_{r,i+1/2,j} = \frac{D_{r,i+1/2,j}}{\Delta r} (n_{i,j} G(\alpha_{i+1/2,j}^r) - n_{i+1,j} F(\alpha_{i+1/2,j}^r)), \quad (8)$$

$$\phi_{z,i,j+1/2} = \frac{D_{z,i,j+1/2}}{\Delta z_j} (n_{i,j} G(\alpha_{i,j+1/2}^z) - n_{i,j+1} G(\alpha_{i,j+1/2}^z)), \quad (9)$$

where

$$\alpha_{i+1/2,j}^r = -s \frac{\mu_{r,i+1/2,j}}{D_{r,i+1/2,j}} (V_{i+1,j} - V_{i,j}), \quad (10)$$

$$\alpha_{i,j+1/2}^z = -s \frac{\mu_{z,i,j+1/2}}{D_{z,i,j+1/2}} (V_{i,j+1} - V_{i,j}). \quad (11)$$

(with $s = -1$ for the electrons and $s = 1$ for the ions) and

$$F(x) = \frac{x}{\exp[x] - 1}, \quad G(x) = \frac{x \exp[x]}{\exp[x] - 1}.$$

Discretized form of the Poisson equation is

$$\begin{aligned} & \left(-2 - \frac{(\Delta r)^2 (\Delta z_{j-1} + \Delta z_j)}{\delta z_{j-1/2} \Delta z_{j-1} \Delta z_j} \right) V_{i,j}^{k+1} \\ & + \frac{(\Delta r)^2}{\delta z_{j-1/2} \Delta z_{j-1}} V_{i,j-1}^{k+1} + \frac{(\Delta r)^2}{\delta z_{j-1/2} \Delta z_j} V_{i,j+1}^{k+1} \\ & + \left(1 - \frac{1}{2i} \right) V_{i-1,j}^{k+1} + \left(1 + \frac{1}{2i} \right) V_{i+1,j}^{k+1} \\ & - \frac{e}{\epsilon_0} n_0 (\Delta r)^2 n_{e,i,j}^{k+1} + \frac{e}{\epsilon_0} n_0 (\Delta r)^2 n_{p,i,j}^{k+1} = 0, \\ & (i = 1, 2, \dots, N_r - 1; j = 1, 2, \dots, N_z - 1), \end{aligned} \quad (12)$$

while along direction $r = 0$ is

$$\begin{aligned} & \left(-4 - \frac{(\Delta r)^2 (\Delta z_{j-1} + \Delta z_j)}{\delta z_{j-1/2} \Delta z_{j-1} \Delta z_j} \right) V_{0,j}^{k+1} + 4V_{1,j}^{k+1} \\ & + \frac{(\Delta r)^2}{\delta z_{j-1/2} \Delta z_{j-1}} V_{0,j-1}^{k+1} + \frac{(\Delta r)^2}{\delta z_{j-1/2} \Delta z_j} V_{0,j+1}^{k+1} \\ & - \frac{e}{\epsilon_0} n_0 (\Delta r)^2 n_{e,0,j}^{k+1} + \frac{e}{\epsilon_0} n_0 (\Delta r)^2 n_{p,0,j}^{k+1} = 0, \\ & (j = 1, 2, \dots, N_z - 1). \end{aligned} \quad (13)$$

Discretized set of coupled equations connects concentrations and potential at time $(k+1)\Delta t$ with values of concentrations and potential at time $k\Delta t$. Since system of algebraic equations (7)-(13) is non-linear we will solve it by applying the Newton–Raphson algorithm [3]. Linearizing the system by introducing a vector $\mathbf{u} = (n_e, n_p, V)^T$ and a correction $\delta \mathbf{u}$ of the same vector (during Newton-Raphson iterations), we obtain a set of linear equations for the correction vector:

$$\begin{aligned} & \hat{a}_{i,j} \delta \mathbf{u}_{i-1,j} + \hat{b}_{i,j} \delta \mathbf{u}_{i,j} + \hat{c}_{i,j} \delta \mathbf{u}_{i+1,j} \\ & + \hat{d}_{i,j} \delta \mathbf{u}_{i,j-1} + \hat{e}_{i,j} \delta \mathbf{u}_{i,j+1} = \mathbf{f}_{i,j}, \\ & (i = 0, 1, \dots, N_r - 1; j = 1, 2, \dots, N_z - 1). \end{aligned} \quad (14)$$

where \hat{a} denotes that a is a 3×3 matrix. Components of the matrices from the previous equation are long expressions and can be obtained straightforwardly. Equation (14) is computationally very demanding and one has to solve it very efficiently in order to get solutions of the fluid equations in a reasonable time. Having in mind that fluid solver is usually combined with Monte Carlo simulation in hybrid models, and that after every cycle of Monte Carlo simulation one solves the set of fluid equations, the importance of the efficiency is evident.

From known values of n_e, n_p, V at $k\Delta t$ we calculate the values at $(k+1)\Delta t$ by solving (14). After that we iterate (7)-(13) through time until the steady concentrations are obtained.

Since neither standard algorithms (e.g. Gauss elimination, LU decomposition) nor iterative algorithms (Gauss-Seidel, Jacobi, SOR)[3] are efficient enough, we have applied the multigrid method [4] to solve (14). The latter method takes $\mathcal{O}(N)$ operation for a linear system with N unknowns, while the former take at least $\mathcal{O}(N^2)$. Typically 80×80 or even coarser grids were used so far while we can use much finer grids.

Moreover we have developed an improvement of the standard multigrid algorithm. The main idea consist of solving system (14) on smaller discretization grid $N_r \times N_z$, and then for the grid $2N_r \times 2N_z$ as an initial solution to take extrapolated stationary solution from $N_r \times N_z$ and long integration time step. In such way we go to finer and finer grids, reaching the wanted number of grid points in the end (the finest one).

The solution on $N_r \times N_z$ was obtained taking arbitrary initial n_e, n_p and V and the initial time step was usually $\Delta t_1 = 1ns$ (or any time for which the system (14) is convergent). After each time integration step Δt_k , new time integration step is

$\Delta t_{k+1} = n\Delta t_k$ (usually $n = 5$). It turns out that we can take greater and greater integration time steps as we approach the stationary solution. However if t_{k+1} is too large (the norm of a correction vector in Newton-Raphson iteration exceeds some upper limit and the system is not robust for that time step), we go back and choose $\Delta t_{k+1} = \Delta t_k$. In such way we approach the stationary solution very fast. We call our method multilevel prolongation method.

3. Results

On the basis of glow discharge measurements in argon in cylindrical geometry with $I = 920 \mu A$, $V = 255.9 V$; $d = 1.1 cm$, $R = 2.7 cm$, $pd = 75 Pa \cdot cm$ ($p = 0.514 torr$)[6], we have obtained an analytic form for the source terms $S_p(r, z) = 0.35 * 10^{22} * \frac{(\frac{z}{L})^2 \exp(-50(\frac{z}{L})^8)}{1 + \exp(a\frac{r}{R} - b)} m^{-3}s^{-1}$, $S_e(r, z) = 1.75 * 10^{22} * \frac{(\frac{z}{L} - 0.5) \exp(-40(\frac{z}{L} - 0.5)^2) \theta(\frac{z}{L} - 0.5)}{1 + \exp(a\frac{r}{R} - b)} m^{-3}s^{-1}$.

Changing the parameters a and b one may obtain different radial profiles which correspond to the cases of constricted and non-constricted discharge. Other input parameters are $\mu_e = \frac{30}{p} m^2 V^{-1} s^{-1}$ where p is the pressure given in *torr*; $D_e = \mu_e \frac{kT_e}{e}$ with $kT_e = 1 eV$; μ_p was taken from [7]; $D_e = \mu_p \frac{kT_p}{e}$ with $kT_p = 0.026 eV$. The boundary conditions are $V(r, 0) = 0$; $V(r, d) = 255.9 V$; $n_e(r, 0) = n_e(r, d) = 0$; $n_p(r, 0) = n_p(r, d) = 0$; $V(R, l)$ along the walls is interpolated linearly; $n_e = n_p = 0$ along the walls.

We have carried out calculations on a personal computer with processor Athlon 3200+ and 512 Mb of RAM memory.

Number of Newton-Raphson iterations during the solving of nonlinear system was less than 10. Newton-Raphson iterations are stopped when the sum of the corrections was less than 10^{-6} . Time evolution are stopped when the relative change in densities become less than 10^{-6} . The overall integration time for the stationary solution was of the order of 1s which is unimportant for our algorithm which advances through time by a factor n .

Execution times are given in Fig.1. We can easily see that the slope of the multigrid solvers (without (M) and with our acceleration (M+L)) is different that for the iterative method which confirms different efficiencies of these methods.

Fig.2–Fig.4 and Fig.5–Fig.7 show the solution for $a = 30, b = 24$ and $a = 10, b = 1$, respectively. We can see in Fig.4, Fig.7 that the electron and ion densities are highly sensitive to the grid size. In the first case both densities increase with the grid, while

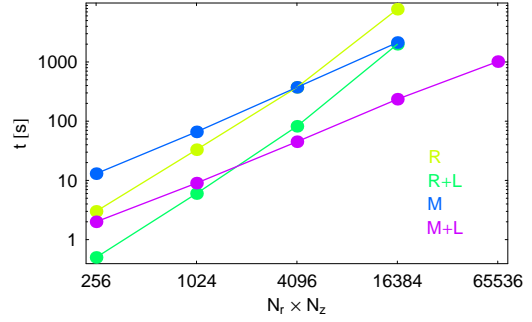


Figure 1: Execution times in seconds for different integration strategies. R denotes results obtained by iterative algorithm, M by multigrid, while L denotes multilevel prolongation method. Grids have $N_r = N_z$.

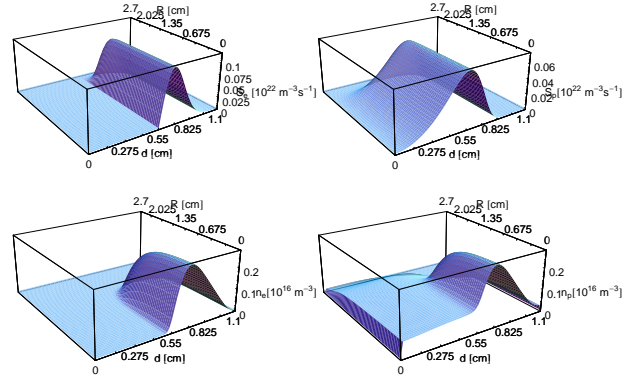


Figure 2: Source terms and densities for $a = 30$, $b = 24$ for grid size 64×64 .

in the second case the electron density decreases. The ion current to the cathode in the first case is $I = 0.59 mA$ and in the second case $I = 0.035 mA$ and are only very weakly dependant of the grid size.

4. Conclusions

We have developed an efficient method for 2D fluid equations in cylindrical geometry. We have applied the multigrid to our knowledge for the first time to solve a system of equations for an obstructed dc glow discharge and with implementation for multilevel prolongation approach. Tremendous acceleration in respect to the iterative methods is obtained by applying multigrid method combined with multilevel prolongation method. From the solution we may conclude importance of the grid size: is not so important for the ion flux to the cathode, but for densities it is important.

A question which arises is how fine grid may be imposed by the physics of the problem. The answer should be probably not finer than the mean

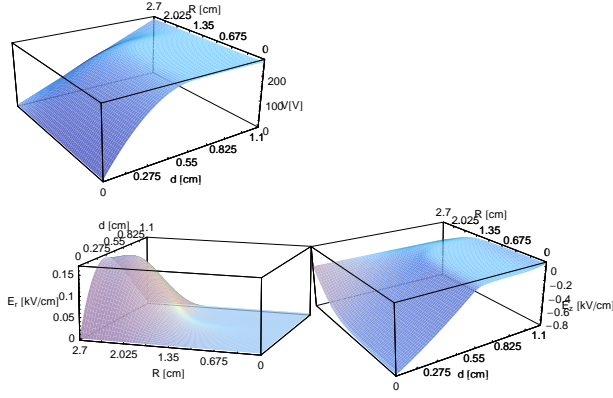


Figure 3: Potential and electric field for $a = 30$, $b = 24$ for grid size 64×64 .

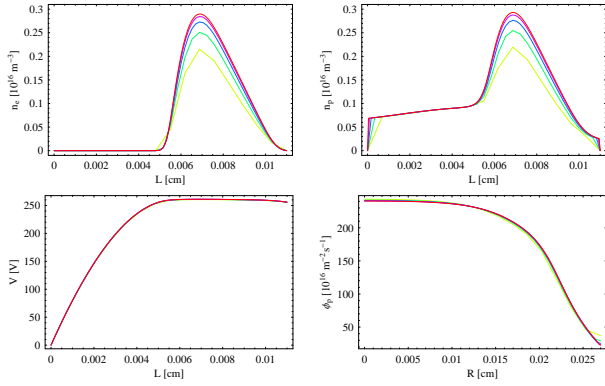


Figure 4: Potential and electric field for $a = 30$, $b = 24$.

free path for the ionization which may vary with the external parameters of the discharge.

5. References

- [1] J. D. P. Passchier, Numerical Fluid Models for RF discharges, PhD Thesis, Utrecht, 1994.
- [2] A. Fiala, L. C. Pitchford, J. P. Boeuf, Phys. Rev. E **49** (1994) 5607.
- [3] W. H. Press, S. A. Teukolsky, W. T. Vetterling, B. P. Flannery, *Numerical Recipes in C*, Second Edition (Cambridge University Press, 1992).
- [4] U. Trottenberg, C. W. Oosterlee, A. Schüller, *Multigrid*, (academic press, 2001).
- [5] Z. Donkó, private communication.
- [6] D. Marić et al, J. Phys. D: Appl. Phys. **36** (2003) 2639.
- [7] A. V. Phelps, Z. Lj. Petrović, Plasma Sources Sci. Technol. **8** (1999) R21.

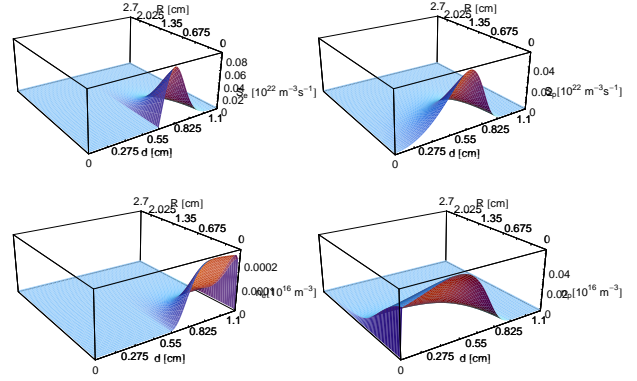


Figure 5: Source terms and densities for $a = 10$, $b = 1$ for grid size 64×64 .

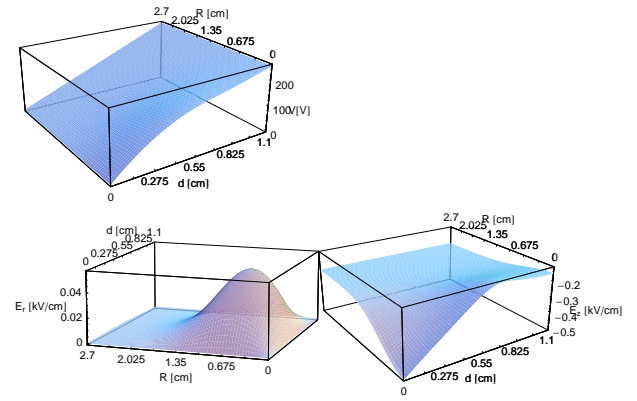


Figure 6: Potential and electric field for $a = 10$, $b = 1$ for grid size 64×64 .

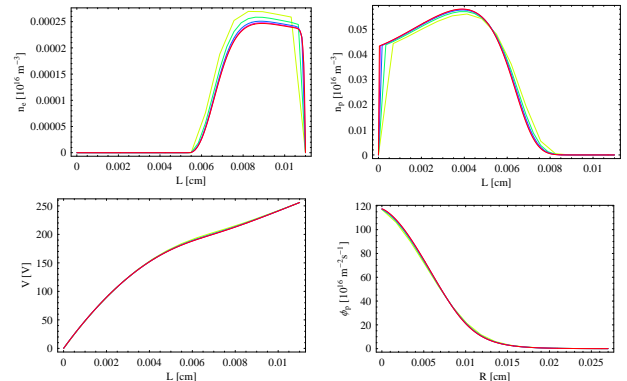


Figure 7: Potential and electric field for $a = 10$, $b = 1$.